Computerized Radiographic Mass Detection—Part I: Lesion Site Selection by Morphological Enhancement and Contextual Segmentation

Huai Li, Yue Wang, K. J. Ray Liu*, Shih-Chung B. Lo, and Matthew T. Freedman

***Abstract*—This paper presents a statistical model supported approach for enhanced segmentation and extraction of suspicious mass areas from mammographic images. With an appropriate statistical description of various discriminate characteristics of both true and false candidates from the localized areas, an improved mass detection may be achieved in computer-assisted diagnosis (CAD). In this study, one type of morphological operation is derived to enhance disease patterns of suspected masses by cleaning up unrelated background clutters, and a model-based image segmentation is performed to localize the suspected mass areas using stochastic relaxation labeling scheme. We discuss the importance of model selection when a finite generalized Gaussian mixture is employed, and use the information theoretic criteria to determine the optimal model structure and parameters. Examples are presented to show the effectiveness of the proposed methods on mass lesion enhancement and segmentation when applied to mammographical images. Experimental results demonstrate that the proposed method achieves a very satisfactory performance as a preprocessing procedure for mass detection in CAD.**

***Index Terms*—Finite mixture, image enhancement, image segmentation, information criterion, morphological filtering, relaxation labeling.**

I. Introduction

In RECENT years, several computer-assisted diagnosis (CAD) schemes for mass detection and classification have been developed [1]–[13]. Though it may be difficult to compare the relative performance of these methods, because the reported performance strongly depends on the degree of subtlety of masses in the selected database, accurate selection of suspected masses is considered a critical and first step due to the variability of normal breast tissue and the lower contrast and ill-defined margins of masses [3], [6], and since no subtle masses should be missed before any further analysis.

A number of image processing techniques have been proposed to perform suspicious mass site selection. Kobatake *et al.* [1] proposed using a iris filter to detect tumors as suspicious regions with very weak contrast to their background. Sameti *et al.* [7] used fuzzy sets to partition the mammographic image data. Lau and Yin *et al.* independently proposed using bilateral-subtraction to determine possible mass locations [9], [13]. Some other investigators proposed using pixel-based feature segmentation of spiculated masses [4], [8]. Kegelmeyer has reported promising results for detecting spiculated tumors based on local edge characteristics and Laws texture features [8]. Karssemeijer *et al.* [4] proposed to identify stellate distortions by using the orientation map of line-like structures. Recently, Petrick *et al.* [6] proposed a two-stage adaptive density-weighted contrast enhancement filtering technique along with edge detection and morphological feature classification for automatic segmentation of potential masses. Kupinski and Giger [3] presented a radial gradient index-based algorithm and a probabilistic algorithm for seeded lesion segmentation.

Nevertheless, to our best knowledge, few work has been dedicated to improve the task of lesion site selection although it is indeed a very crucial step in CAD. Especially, few studies have used and justified model-based image processing techniques for unsupervised lesion site selection [11]. Zwiggelaar *et al.*developed a statistical model to describe and detect the abnormal pattern of linear structures of spiculated lesions [2]. In their work, the probability density function of the observation vectors for each class is assumed to be normal. we have experienced that the "normal" distribution for each class is nor true. Li *et al.* proposed using a Markov random field model to extract suspicious masses for mass detection [11]. In their study, most of model parameters were chosen empirically, and the mammogram was segmented into three regions (background, fat, and parenchymal or tumors).

Stochastic model-based image segmentation is a technique for partitioning an image into distinctive meaningful regions based on the statistical properties of both gray level and context images. A good segmentation result would depend on suitable model selection for a specific image modality [16], [17] where model selection refers to the determination of both the number of image regions and the local statistical distributions of each region. Furthermore, a segmentation result would be improved

Manuscript received February 3, 1997; revised January 9, 2001. This work was supported in part by the Department of Defense under Grants DAMD17-98-1-8045 and DAMD17-96-1-6254 through a subcontract from University of Michigan, Ann Arbor, and by the National Science Foundation (NSF) under NYI Award MIP-9457397. The Associate Editor responsible for coordinating the review of this paper and recommending its publication was M. Giger. *Asterisk indicates corresponding author.*

H. Li is with the Electrical Engineering Department and Institute for Systems Research, University of Maryland at College Park, College Park, MD 20742 USA. He is also with the Department of Radiology, Georgetown University Medical Center, Washington, DC 20007 USA.

Y. Wang is with the Department of Electrical Engineering and Computer Science, The Catholic University of America, Washington, DC 20064 USA. He is also with the Department of Radiology, Georgetown University Medical Center, Washington, DC 20007 USA.

*K. J. Ray Liu is with the Electrical Engineering Department and Institute for Systems Research University of Maryland at College Park, College Park, MD 20742 USA (e-mail: kjrliu@eng.umd.edu).

S.-C. B. Lo and M. T. Freedman are with the Department of Radiology, Georgetown University Medical Center, Washington, DC 20007 USA.

Publisher Item Identifier S 0278-0062(01)02831-2.

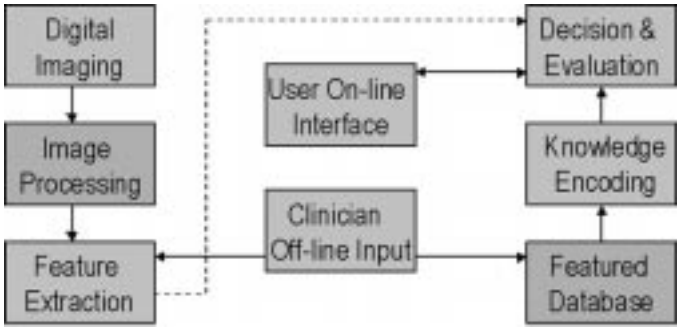

Fig. 1. Major components in CAD.

with preenhanced pattern of interest being segmented. The only assumption for suspected mass site selection is that suspected mass areas should be brighter than the surrounding breast tissues which is valid for most of the real cases. When some masses lie either within an inhomogeneous pattern of fibroglandular tissue or are partially or completely surrounded by fibroglandular tissue, enhancement of mass-related signals is important.

Fig. 1 shows a general block diagram of CAD systems. This paper focuses on "image processing" block, to just automatically pick up all possible lesion sites. We aim on two essential issues in the stochastic model-based image segmentation: enhancement and model selection. Based on the differential geometric characteristics of masses against the background tissues, we propose one type of morphological operation to enhance the mass patterns on mammograms. Then we employ a finite generalized Gaussian mixture (FGGM) distribution to model the histogram of the mammograms where the statistical properties of the pixel images are largely unknown and are to be incorporated. We incorporate the EM algorithm with two information theoretic criteria to determine the optimal number of image regions and the kernel shape in the FGGM model. Finally, we apply a contextual Bayesian relaxation labeling (CBRL) technique to perform the selection of suspected masses. The major differences of our work from the previous work [1]–[6], [8]–[13] are as follows.

1) We present a new algorithm of morphological filtering for image enhancement in which the combined operations are applied to the original gray tone image and the higher sensitive lesion site selection of the enhanced images are observed.
2) We justify and pilot test the FGGM distribution in modeling mammographic pixel images together with a model selection procedure based on the two information theoretic criteria. This allows an automatic identification of both the number (K) and kernel shape (α) of the distributions of tissue types.
3) We develop a new algorithm (CBRL) for segmenting mass areas where the comparable results are achieved as those using Markov random field model-based approaches while with much less computational complexity.

The presentation of this paper is organized as follows. In Section II, the proposed dual morphological operation enhancement technique is described in detail. The theory and algorithm on FGGM modeling, model selection, and parameter estimation are presented in Section III. This is followed by a discussion on the selection of suspicious masses using the CBRL approach. Evaluation results are given and discussed in Section IV. Finally, the paper is concluded by Section V.

II. Morphological Enhancement

One of the main difficulties in suspicious mass segmentation is that mammographic masses are often overlapped with dense breast tissues. Therefore, it is necessary to remove bright background caused by dense breast tissues while preserving the features and patterns related to the masses. For this purpose, background correction is an important step for mass segmentation. We propose a mass pattern-dependent background removal approach using morphological operations.

A. Morphological Filtering Theory

Morphological operations can be employed for many image processing purposes, including edge detection, region segmentation, and image enhancement. The beauty and simplicity of mathematical morphology approach come from the fact that a large class of filters can be represented as the combination of two simple operations: erosion and dilation. Let Z denote the set of integers and $f(i, j)$ denote a discrete image signal, where the domain set is given by $\{i, j\} \in N_1 \times N_2$, $N_1 \times N_2 \subset Z^2$ and the range set by $\{f\} \in N_3$, $N_3 \subset Z$. A structuring element B is a subset in Z^2 with a simple geometrical shape and size. Denote $B^s = \{-b : b \in B\}$ as the symmetric set of B and B_{t_1, t_2} as the translation of B by (t_1, t_2), where $(t_1, t_2) \in Z^2$. The erosion $f \ominus B^s$ and dilation $f \oplus B^s$ can be expressed as [19]

$$(f \ominus B^s)(i, j) = \min_{t_1, t_2 \in B_{i,j}} (f(t_1, t_2)) \tag{1}$$

$$(f \oplus B^s)(i, j) = \max_{t_1, t_2 \in B_{i,j}} (f(t_1, t_2)). \tag{2}$$

On the other hand, opening $f \circ B$ and closing $f \bullet B$ are defined as [19]

$$(f \circ B)(i, j) = ((f \ominus B^s) \oplus B)(i, j) \tag{3}$$

$$(f \bullet B)(i, j) = ((f \oplus B^s) \ominus B)(i, j). \tag{4}$$

A gray value image can be viewed as a two-dimensional surface in a three-dimensional space. Given an image, the opening operation removes the objects, which have size smaller than the structuring element, with positive intensity. Thus, with the specified structuring element, one can extract different image contexts by taking the difference between the original and opening processed image, which is known as "tophat" operation [19].

B. Morphological Enhancement Algorithms

Based on the properties of morphological filters, we designed one type of mass pattern-dependent enhancement approaches. The algorithm is implemented by dual morphological tophat operations following by a subtraction which is described as follows.

Step 1) The textures without the pattern information of interest are extracted by a tophat operation

$$r_1(i, j) = \max(0, [f(i, j) - (f \circ B_1)(i, j)]) \quad (5)$$

where $f(i, j)$ is the original image, and $r_1(i, j)$ is the residue image between the original image and the opening of the original image by a specified structuring element B_1. The size of B_1 should be chosen smaller than the size of masses.

Step 2) Let $r_2(i, j)$ be the mass pattern enhanced image by background correction, i.e., by the second tophat operation on $f(i, j)$

$$r_2(i, j) = \max(0, [f(i, j) - (f \circ B_2)(i, j)]) \quad (6)$$

where B_2 is a specified structuring element which has a larger size than masses.

Step 3) The enhanced image $f_1(i, j)$ can be derived as

$$f_1(i, j) = \max(0, [r_2(i, j) - r_1(i, j)]). \quad (7)$$

This operation is called "dual morphological operation." It can remove the background noise and the structure noise inside the suspected mass patterns. Fig. 2 shows the mass patch and the enhanced results of each step using the dual morphological operation. As we can see from Fig. 2, both background correction [Fig. 2(c)] and dual morphological operation [Fig. 2(d)] enhanced the mass pattern, but dual morphological operation removed more structural noise inside the mass region which in turn would improve the mass segmentation results.

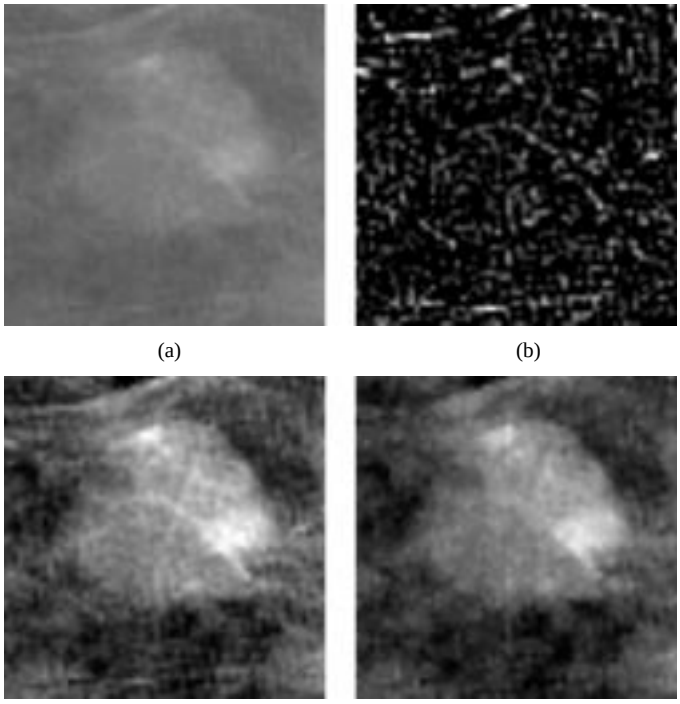

Fig. 2. Original and enhancement result of the mass patch using dual-morphological operation. (a) Original image block $f(i, j)$. (b) Textures $r_1(i, j)$. (c) Background correction result $r_2(i, j)$. (d) Enhanced result $f_1(i, j)$.

III. Model-Based Segmentation

A. Statistical Modeling

Given a digital image consisting of $N_1 \times N_2$ pixels, assume this image contains K regions. By randomly reordering all pixels in the underlying probability space, one can treat pixel labels as random variables and introduce a prior probability measure π_k. Then the FGGM probability density function (pdf) of gray level of each pixel is given by [17]

$$p(x_i) = \sum_{k=1}^{K} \pi_k p_k(x_i), \qquad i = 1, \ldots, N_1 N_2, \quad x_i = 0, 1, \ldots, L-1 \quad (8)$$

where x_i is the gray level of pixel i, and L is the number of gray levels. $p_k(x_i)$s are conditional region pdfs with the weighting factor π_k, satisfying $\pi_k > 0$, and $\sum_{k=1}^{K} \pi_k = 1$. The generalized Gaussian pdf given region k is defined by

$$p_k(x_i) = \frac{\alpha \beta_k}{2\Gamma(1/\alpha)} \exp[-|\beta_k(x_i - \mu_k)|^{\alpha}], \qquad \alpha > 0,$$

$$\beta_k = \frac{1}{\sigma_k} \left[\frac{\Gamma(3/\alpha)}{\Gamma(1/\alpha)}\right]^{1/2}. \quad (9)$$

where μ_k is the mean, $\Gamma(\cdot)$ is the Gamma function. β_k is a parameter related to the variance σ_k. It can be shown that when $\alpha = 2.0$, one has the Gaussian pdf; when $\alpha = 1.0$, one has the Laplacian pdf. When $\alpha \gg 1$, the distribution tends to a uniform pdf; when $\alpha < 1$, the pdf becomes sharp. Therefore, the generalized Gaussian model is a suitable model to fit the histogram distribution of those images whose statistical properties are unknown since the kernel shape can be controlled by selecting different α values.

The whole image can be well approximated by an independent and identically distributed random field $\mathbf{X}$. The corresponding joint pdf is

$$P(\mathbf{x}) = \prod_{i=1}^{N_1 N_2} \sum_{k=1}^{K} \pi_k p_k(x_i) \quad (10)$$

where $\mathbf{x} = [x_1, x_2, \ldots, x_{N_1 N_2}]$, and $\mathbf{x} \in \mathbf{X}$. $p_k(x_i)$ is given in (9). Based on the joint probability measure of pixel images, the likelihood function under FGGM modeling can be expressed as $\mathcal{L}(\mathbf{r}) = \prod_{i=1}^{N_1 N_2} p_{\mathbf{r}}(x_i)$ where $\mathbf{r} : \{K, \alpha, \pi_k, \mu_k, \sigma_k, k = 1, \ldots, K\}$ denotes the model parameter set.

B. Model Identification

With an appropriate system likelihood function, the objective of model identification is to estimate the model parameters by maximizing the likelihood function, or equivalently minimizing the relative entropy between the image histogram $p_{\mathbf{x}}(u)$ and the estimated pdf $p_{\mathbf{r}}(u)$, where u is the gray level. Based on the FGGM model, the EM algorithm is applied to estimate the model parameters. The EM algorithm is an iterative technique for maximum-likelihood (ML) estimation [20]. Recently, it has been used in many medical imaging applications [15]. Instead

of evaluating directly the value of ML, we use the global relative entropy (GRE) between the histogram and the estimated FGGM distribution to measure the performance of parameter estimation, given by

$$\mathrm{GRE}(p_{\mathbf{x}}||p_{\mathbf{r}}) = \sum_{u} p_{\mathbf{x}}(u) \log \frac{p_{\mathbf{x}}(u)}{p_{\mathbf{r}}(u)}. \tag{11}$$

Motivated by the same spirit of conventional EM algorithm for finite normal mixtures (FNMs), we formulated the EM algorithm to estimate the parameter values of the FGGM. The algorithm is summarized as follows.

EM Algorithm:

1) For $\alpha = \alpha_{\min}, \ldots, \alpha_{\max}$
   - $m = 0$, given initialized $\mathbf{r}^{(0)}$
   - E-step: for $i = 1, \ldots, N_1N_2$, $k = 1, \ldots, K$, compute the probabilistic membership

$$z_{ik}^{(m)} = \frac{\pi_k^{(m)} p_k(x_i)}{\sum_{k=1}^{K} \pi_k^{(m)} p_k(x_i)}. \tag{12}$$

   - M-step: for $k = 1, \ldots, K$, compute the updated parameter estimates

$$\begin{cases} \pi_k^{(m+1)} = \dfrac{1}{N_1N_2} \displaystyle\sum_{i=1}^{N_1N_2} z_{ik}^{(m)} \\ \mu_k^{(m+1)} = \dfrac{1}{N_1N_2\pi_k^{(m+1)}} \displaystyle\sum_{i=1}^{N_1N_2} z_{ik}^{(m)} x_i \\ \sigma_k^{2(m+1)} = \dfrac{1}{N_1N_2\pi_k^{(m+1)}} \displaystyle\sum_{i=1}^{N_1N_2} z_{ik}^{(m)} (x_i - \mu_k^{(m+1)})^2. \end{cases} \tag{13}$$

   - When $|\mathrm{GRE}^{(m)}(p_{\mathbf{x}}||p_{\mathbf{r}}) - \mathrm{GRE}^{(m+1)}(p_{\mathbf{x}}||p_{\mathbf{r}})| \le \epsilon$ is satisfied, go to Step 2 Otherwise, $m = m+1$ and go to E-Step.
2) Compute GRE, and go to Step 1.
3) Choose the optimal $\hat{\mathbf{r}}$ which corresponds to the minimum GRE.

As we mentioned in Section I, the two important parameters in model selection are K and α. Determination of the region parameter K directly affects the quality of the resulting model parameter estimation and in turn, affects the result of segmentation. In this paper we propose an approach to determine the value of K based on two popular information theoretic criteria introduced by Akaike [23] and by Rissanen [24]. Akaike proposed to select the model that gives the minimum Akaike information criterion (AIC), defined by

$$\mathrm{AIC}(K) = -2\log(\mathcal{L}(\hat{\mathbf{r}}_{ML})) + 2K' \tag{14}$$

where $\hat{\mathbf{r}}_{ML}$ is the ML estimate of the model parameter set $\mathbf{r}$, and K' is the number of free adjustable parameters in the model [15], [23]. AIC criterion will select the correct number of the image regions K_0 when

$$K_0 = \arg\left\{ \min_{1 \le K \le K_{\mathrm{MAX}}} \mathrm{AIC}(K) \right\}. \tag{15}$$

Rissanen addressed the problem from a quite different point of view. Rissanen reformulated the problem explicitly as an information coding problem in which the best model fitness is measured such that it assigns high probabilities to the observed data while at the same time the model itself is not too complex to describe [24]. The model is selected by minimizing the total description length defined by minimum description length (MDL)

$$MDL(K) = -\log(\mathcal{L}(\hat{\mathbf{r}}_{ML})) + 0.5K' \log(N_1N_2). \tag{16}$$

Similarly, the correct number of the distinctive image regions K_0 will be estimated when

$$K_0 = \arg\left\{ \min_{1 \le K \le K_{\mathrm{MAX}}} MDL(K) \right\}. \tag{17}$$

C. Bayesian Relaxation Labeling

Once the FGGM model is given, a segmentation problem is the assignment of labels to each pixel in the image. A straightforward way is to label pixels into different regions by maximizing the individual likelihood function $p_k(x)$. This approach is called ML classifier, which is equivalent to a multiple thresholding method. Usually, this method may not achieve a good performance since there is lack of local neighborhood information to be included to make a good decision. CBRL algorithm [25] is one of the approaches, which can incorporate the local neighborhood information into labeling procedure and thus improve the segmentation performance. In this study, we developed the CBRL algorithm to perform/refine pixel labeling based on the localized FGGM model, which is defined as follows.

Let ∂i be the neighborhood of pixel i with an $m \times m$ template centered at pixel i. An indicator function is used to represent the local neighborhood constraints $R_{ij}(l_i, l_j) = I(l_i, l_j)$, where l_i and l_j are labels of pixels i and j, respectively. Note that pairs of labels are now either compatible or incompatible. Similar to reference [25], one can compute the frequency of neighbors of pixel i which has the same label values k as at pixel i

$$\pi_k^{(i)} = p(l_i = k|\mathbf{l}_{\partial i}) = \frac{1}{m^2 - 1} \sum_{j \in \partial i,\, j \ne i} I(k, l_j) \tag{18}$$

where $\mathbf{l}_{\partial i}$ denotes the labels of the neighbors of pixel i. Since $\pi_k^{(i)}$ is a conditional probability of a region, the localized FGGM pdf of gray level x_i at pixel i is given by

$$p(x_i|\mathbf{l}_{\partial i}) = \sum_{k=1}^{K} \pi_k^{(i)} p_k(x_i) \tag{19}$$

where $p_k(x_i)$ is given in (9). Assuming gray values of the image are conditional independent, the joint pdf of $\mathbf{x}$, given the context labels $\mathbf{l}$, is

$$P(\mathbf{x}|\mathbf{l}) = \prod_{i=1}^{N_1N_2} \sum_{k=1}^{K} \pi_k^{(i)} p_k(x_i) \tag{20}$$

where $\mathbf{l} = (l_i : i = 1, \ldots, N_1N_2)$.

It is known that CBRL algorithm can obtain a consistent labeling solution based on the localized FGGM model (19). Since

TABLE I
DISTRIBUTION OF THE EFFECTIVE SIZE OF THE 186 MASSES USED IN THIS STUDY. THE EFFECTIVE SIZE IS DEFINED AS THE SQUARE ROOT OF THE PRODUCT OF THE MAXIMUM AND MINIMUM DIAMETERS OF THE MASS

	$0-5mm$	$6-10mm$	$11-15mm$	$16-20mm$	$21-25mm$	$26-30mm$
#	3	55	78	29	17	4

$\mathbf{l}$ represents the labeled image, it is consistent if $S_i(l_i) \geq S_i(k)$, for all $k = 1, \ldots, K$ and for $i = 1, \ldots, N_1N_2$ [25], where

$$S_i(k) = \pi_k^{(i)} p_k(x_i). \tag{21}$$

Now we can define

$$A(\mathbf{l}) = \sum_{i=1}^{N_1N_2} \left(\sum_k I(l_i, k) S_i(k) \right) \tag{22}$$

as the average measure of local consistency, and

$$LC_i = \sum_k I(l_i, k) S_i(k), \qquad i = 1, \ldots, N_1N_2 \tag{23}$$

represents the local consistency based on $\mathbf{l}$. The goal is to find a consistent labeling $\mathbf{l}$ which can maximize (22). In the real application, each local consistency measure LC_i can be maximized independently. In [25], it has been shown that when $R_{ij}(l_i, l_j) = R_{ji}(l_j, l_i)$, if $A(\mathbf{l})$ attains a local maximum at $\mathbf{l}$, then $\mathbf{l}$ is a consistent labeling.

Based on the localized FGGM model, $l_i^{(0)}$ can be initialized by ML classifier

$$l_i^{(0)} = \arg\left\{ \max_k p_k(x_i) \right\}, \qquad k = 1, \ldots, K. \tag{24}$$

Then, the order of pixels is randomly permutated and each label l_i is updated to maximize LC_i, i.e., classify pixel i into kth region if

$$l_i = \arg\left\{ \max_k \pi_k^{(i)} p_k(x_i) \right\}, \qquad k = 1, \ldots, K \tag{25}$$

where $p_k(x_i)$ is given in (9), $\pi_k^{(i)}$ is given in (18). By considering (24) and (25),we developed a modified CBRL algorithm as follows.

CBRL Algorithm:

1) Given $\mathbf{l}^{(0)}$, $m = 0$
2) Update pixel labels
   - Randomly visit each pixel for $i = 1, \ldots, N_1N_2$
   - Update its label l_i according to

$$l_i^{(m)} = \arg\left\{ \max_k \pi_k^{(i)(m)} p_k(x_i) \right\}.$$

3) When

$$\frac{\sum (\mathbf{l}^{(m+1)} \oplus \mathbf{l}^{(m)})}{N_1N_2} \leq 1\%,$$

stop; otherwise, $m = m + 1$, and repeat Step 2.

IV. EXPERIMENTAL RESULTS AND DISCUSSION

In this section, we present the results of using the morphological filtering and model-based segmentation approach we have introduced for enhancement and segmentation of suspicious masses in mammographic images. In addition to the qualitative assessment by the radiologists, we introduce several objective measures to assess the performance of the algorithms we have proposed for enhancement and segmentation.

A testing data set of 200 mammograms and two simulated tone images were used to test and evaluate the performance of the algorithms in this study. The mammograms were selected from the Mammographic Image Analysis Society (MIAS) database and the Brook Army Medical Center (BAMC) database created by the Department of Radiology at Georgetown University Medical Center. Of the 200 mammograms, 50 mammograms are normal, and each of the 150 abnormal mammograms contains at least one mass case of varying size, subtlety, and location. The areas of suspicious masses were identified by an expert radiologist based on visual criteria and biopsy proven results. The total data set includes 113 benign and 73 malignant masses. The distribution of the masses in terms of size is shown in Table I. The BAMC films were digitized with a laser film digitizer (Lumiscan 150) at a pixel size of 100 μm$\times$ 100 μm and 4096 gray levels (12 bits). Before the method was applied the digital mammograms were smoothed by averaging 4×4 pixels into one pixel. According to radiologists, the size of small masses is 3–15 mm in effective diameter. A 3-mm object in an original mammogram occupies 30 pixels in a digitized image with a 100-μm resolution. After reducing the image size by four times, the object will occupy the range of about seven to eight pixels. The object with the size of seven pixels is expected to be detectable by any computer algorithm. Therefore, the shrinking step is applicable for mass cases and can save computation time.

Experimental Evaluation of Morphological Enhancement: In order to justify the suitability of morphological structural elements, the geometric properties of the contexts and textures in mammograms were studied. The basic idea is to keep all mass-like objects within certain size range and remove all others by using the proposed morphological filters with specific structural elements. At the resolution of 400 μm, a disk with a diameter of seven pixels was chosen as the morphological structuring elements B_1 to extract textures in mammograms. Since the smallest masses have seven pixels in diameter with the resolution of 400 μm, this procedure would not destroy mass information. For the purpose of background correction, a disk with a diameter of 75 pixels was used as the morphological structuring element B_2. An object with a diameter of 75 pixels corresponds to 30 mm in the original mammogram. This indicates that all masses with sizes up to 30 mm can be enhanced by background correction. Masses larger than 30 mm are rare cases in the clinical setting. In the last stage of our approach, we applied morphological opening and closing filtering using a disk with a diameter of five to eliminate small objects which also contribute to texture noise.

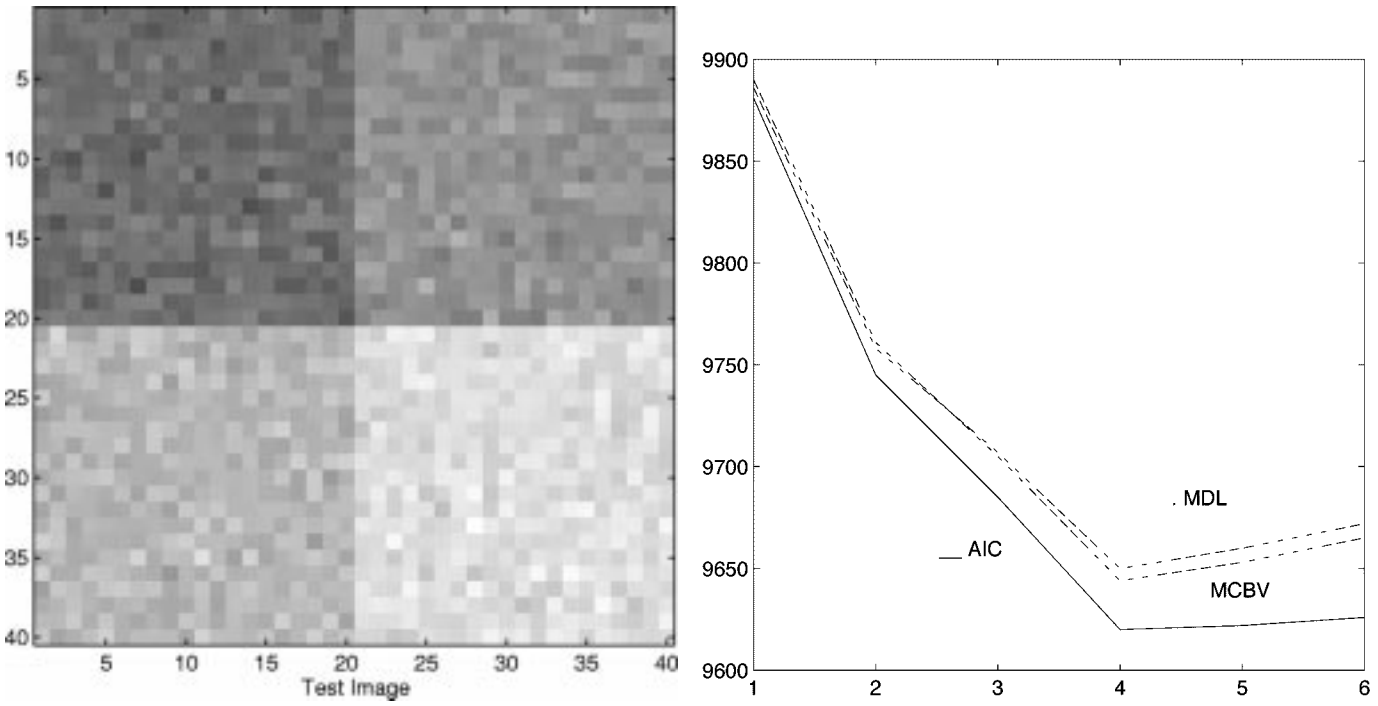

(a) (b)

Fig. 3. (a) Original simulated test image for model selection ($k_0 = 4$, SNR $= 10$ dB) and (b) the AIC/MDL curves in model selection ($\sigma = 30$).

All testing mammograms were processed using the proposed enhancement approach with the suggested structuring element B_1 and B_2. Fig. 5 shows processed mammogram examples using the morphological enhancement. Compared the enhanced results [Fig. 5(b) and (d)] with the original mammograms [Fig. 5(a) and (c)], the proposed method not only enhanced all suspected mass patterns and reduced the texture noise, but also removed the background noise. In summary, the proposed morphological enhancement approach can enhance mass patterns and remove texture structure noises. For dense mammograms, such as the second example in Fig. 5(c) and (d), the mass is obscured by dense fibroglandular tissues, our experience shows applying the dual morphological operation to remove the fibroglandular tissue background is useful. In addition to the visual evaluation by the radiologist, we performed the segmentation to assess the effectiveness of the morphological filtering, based on the enhanced mammograms and the original mammograms.

Simulated Evaluation of Segmentation Algorithms: The performance of model selection using two frequently used methods, i.e., the AIC and MDL [22], were first tested and compared in the simulation study. The computer-generated data was made up of four overlapping normal components. Each component represents one local region. The value for each component were set to a constant value, the noise of normal distribution was then added to this simulation digital phantom. Three noise levels with different variance were set to keep the same signal-to-noise ratio (SNR), where SNR is defined by

$$\text{SNR} = 10 \log_{10} \frac{(\Delta\mu)^2}{\sigma^2} \tag{26}$$

where $\Delta\mu$ is the mean difference between regions, and σ^2 is the noise power. The original data for the simulation study are given in Fig. 3(a). The AIC and MDL curves, as functions of the number of local clusters K, are plotted in Fig. 3(b). According

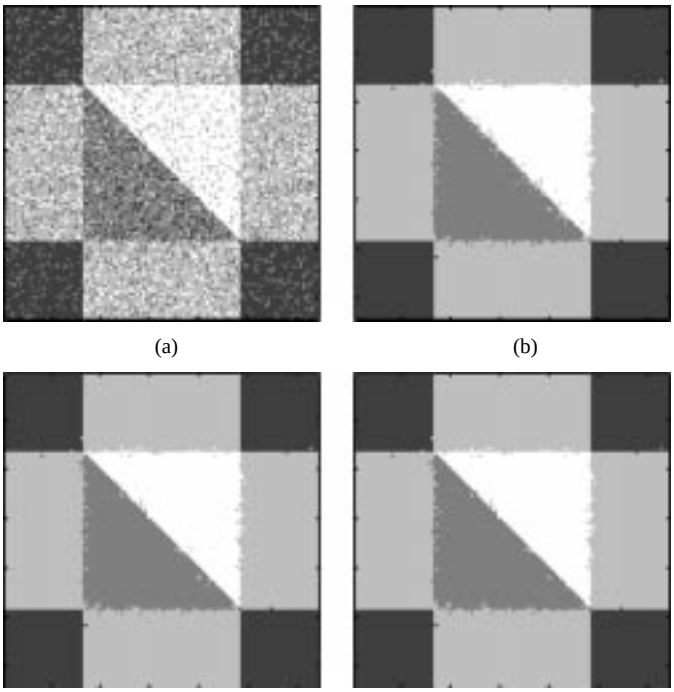

(a) (b) (c) (d)

Fig. 4. Image segmentation by CBRL on simulated image (with initialization by ML classification). (a) ML initialization. (b) First iteration in CBRL. (c) Second iteration in CBRL. (d) Third iteration in CBRL.

TABLE II
COMPARISON OF CBRL, ICM, AND MICM ALGORITHM: SIMULATED DATA

Item	CBRL Result	ICM Result	MICM Result
Classification Error	0.7935%	0.7508%	0.3113%

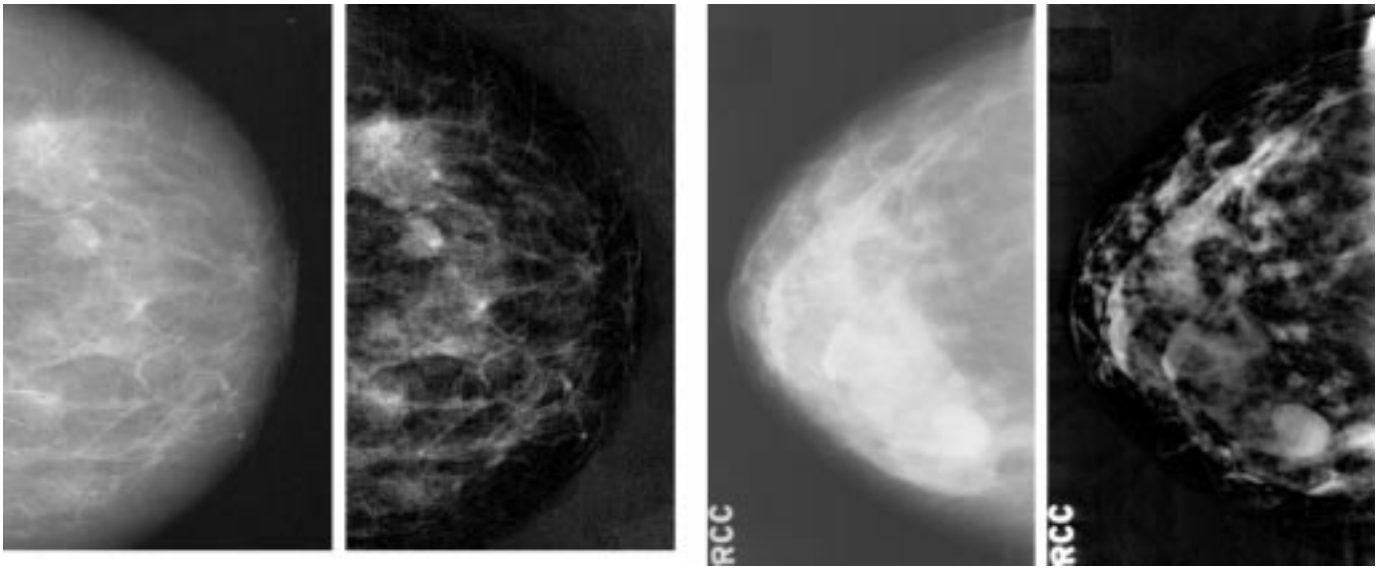

(a) (b) (c) (d)

Fig. 5. Examples of mass enhancement. (a) Original mammogram. (b) Enhanced mammogram. (c) and (d) Another original mammogram and its enhanced result.

to the information theoretic criteria, the minima of these curves indicate the correct number of the local regions. From this experimental figure, it is clear that the number of local regions suggested by these criteria are all correct.

For the validation of image segmentation using CBRL, we apply the algorithm first to a simulated image. We use ML classifier to initialize image segmentation, i.e., to initialize the quantified image by selecting the pixel label with largest likelihood at each node. The classification error after initialization is uniformly distributed over the spatial domain as shown in Fig. 4(a). Our experience suggested this to be a very suitable starting point for contextual relaxation labeling [21]. The CBRL is then performed to fine tune the image segmentation. It should be emphasized that the ground truth is known in this simulated experiment, the percentage of total classification error is used as the criterion for evaluating the performance of segmentation technique. In Fig. 4(a)–(d), the initial segmentation by the ML classification and the stepwise results of three iterations in the CBRL are presented. In this experiment, algorithm initialization results in an average classification error of 30%. It can be clearly seen that a dramatic improvement is obtained after several iterations of the CBRL by using local constraints determined by the context information. In addition, the convergence is fast as one can see, after the first iteration most of the misclassification are removed. We have also implemented two other independent and popular algorithms, namely, the iterated conditional mode (ICM) and the modified iterated conditional mode (MICM) algorithms, so as to assess the comparative performance of the segmentation results among different approaches [21], [22]. The only assumption being made by these three methods is the Markovian property of the context images which can be well justified by the underlying cell oncology and pathology. We have applied these three algorithms to the same testing image and the corresponding classification errors are presented in Table II. The final percentage of classification errors for Fig. 4(d) is 0.7935%. From this experimental comparison, it can be concluded that three algorithms achieved comparable segmentation accuracy and the result produced by the MICM algorithm is most superior, though in terms of computational complexity the CBRL algorithm is the least. It should be noticed that since in MICM algorithm an inhomogeneous configuration of the Markov random field is used, its superior performance is reasonable.

TABLE III
COMPUTED AICS FOR THE FGGM MODEL WITH DIFFERENT α

K	$\alpha = 1.0$	$\alpha = 2.0$	$\alpha = 3.0$	$\alpha = 4.0$
2	651250	650570	650600	650630
3	646220	644770	645280	646200
4	645760	644720	645260	646060
5	645760	644700	645120	646040
6	645740	644670	645110	645990
7	645640	644600	645090	645900
8	645550(min)	644570(min)	645030(min)	645850(min)
9	645580	644590	645080	645880
10	645620	644600	645100	645910

TABLE IV
COMPUTED MDLS FOR THE FGGM MODEL WITH DIFFERENT α

K	$\alpha = 1.0$	$\alpha = 2.0$	$\alpha = 3.0$	$\alpha = 4.0$
2	651270	650590	650630	650660
3	646260	644810	645360	646350
4	645860	644770	645280	646150
5	645850	644770	645280	646100
6	645790	644750	645150	646090
7	645720	644700	645120	645930
8	645680(min)	644690(min)	645100(min)	645900(min)
9	645710	644710	645140	645930
10	645790	644750	645180	645960

On Model-Based Segmentation—Real Case Study: In the real case study, we used two information criteria (AIC and MDL) to determine K. Tables III and IV shows the AIC and MDL values with different K and α of the FGGM model based on one original mammogram. As it can be seen from Tables III and IV, although with different α, all AIC and MDL values achieve the minimum when $K = 8$. It indicates that AIC and

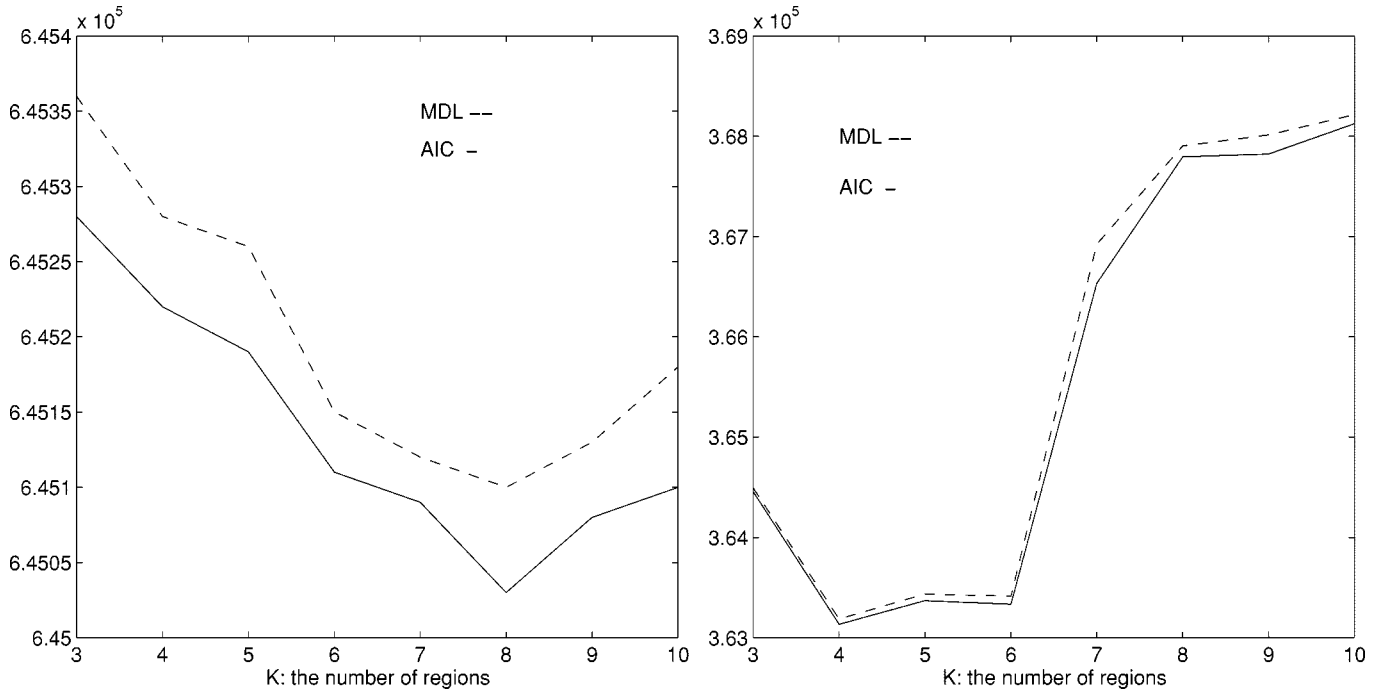

Fig. 6. AIC and MDL curves with different number of region K. (a) Result based on the original mammogram, the optimal $K = 8$. (b) Result based on the enhanced mammogram, the optimal $K = 4$.

MDL are relatively insensitive to the change of α. With this observation, we can decouple the relation between K and α and choose the appropriate value of one while fixing the value of another. Fig. 6(a) and (b) are two examples of AIC and MDL curves with different K and fixed $\alpha = 3.0$. Fig. 6(a) is based on the original mammogram and Fig. 6(b) is based on the enhanced mammogram. As we can see in Fig. 6(a), both criteria achieved the minimum when $K = 8$. It should be noticed that though no ground truth is available in this case, our extensive numerical experiments have shown a very consistent performance of the model selection procedure and all the conclusions were strongly supported by the previous independent work reported by [14]. Fig. 6(b) indicates that $K = 4$is the appropriate choice for the mammogram enhanced by dual morphological operation. This is believed to be reasonable since the number of regions decrease after background correction.

We fixed $K = 8$, and changed the value of α for estimating the FGGM model parameters using the proposed EM algorithm with the original mammogram The GRE value between the histogram and the estimated FGGM distribution was used as a measure of the estimation bias. We found that GRE achieved a minimum distance when the FGGM parameter $\alpha = 3.0$ as shown in Fig. 7. The similar result was shown when we applied the EM algorithm to the enhanced mammogram with $K = 4$. This indicated that the FGGM model might be better than the FNM model ($\alpha = 2.0$) in modeling mammographic images when the true statistical properties of mammograms are generally unknown, though the FNM has been most often chosen in many previous work [15].

After the determination of all model parameters, every pixel of the image was labeled to a different region (from 1 to K) based on the CBRL algorithm. We then selected the brightest region, which corresponding to label K, plus a criterion of closed isolated area, as the candidate region of suspicious masses. According to the visual inspections by the radiologists, when we use $K-1$ instead of K, the results are over-segmented. For the case of using $K+1$, the results are under-segmented. In order to quantify the performance differences between the different segmentation methods, several groups have suggested that the segmentation results may be compared against radiologists' outlines of the lesions [3]. Though the proposed comparison measures are quantitative, the performance measures are still qualitative, since the reference base (e.g., gold standard by the radiologists) is qualitative, subjective, and imperfect. Therefore, in this model-supported approach, in addition to the visual inspections by the radiologists, we have also introduced an objective measure, the GRE between the histogram of the pixel images $p_{\mathbf{x}}(u)$ and the FGGM of the *segmented* image $p_{\mathbf{x},\mathbf{l}}(u)$ to assess the performance of the segmentation, defined by

$$\mathrm{GRE}(p_{\mathbf{x}}(u)\|p_{\mathbf{x},\mathbf{l}}(u)) = \sum_{u} p_{\mathbf{x}}(u)\log\frac{p_{\mathbf{x}}(u)}{p_{\mathbf{x},\mathbf{l}}(u))} \qquad (27)$$

where $\mathbf{l}$ is the context image estimated by the segmentation algorithm. Considering that the ergodic theorem is the most fundamental principle in the detection and estimation theory, it is believed that when a good segmentation is achieved, the distance between the $p_{\mathbf{x}}(u)$ and $p_{\mathbf{x},\mathbf{l}}(u)$ should be minimized and

TABLE V
COMPARISON OF SEGMANTATION ERROR RESULTING FROM NONCONTEXTUAL AND CONTEXTUAL METHODS

Method	Soft Classification	Bayesian Classification	CBRL
GRE Value	0.0067	0.4406	0.1578

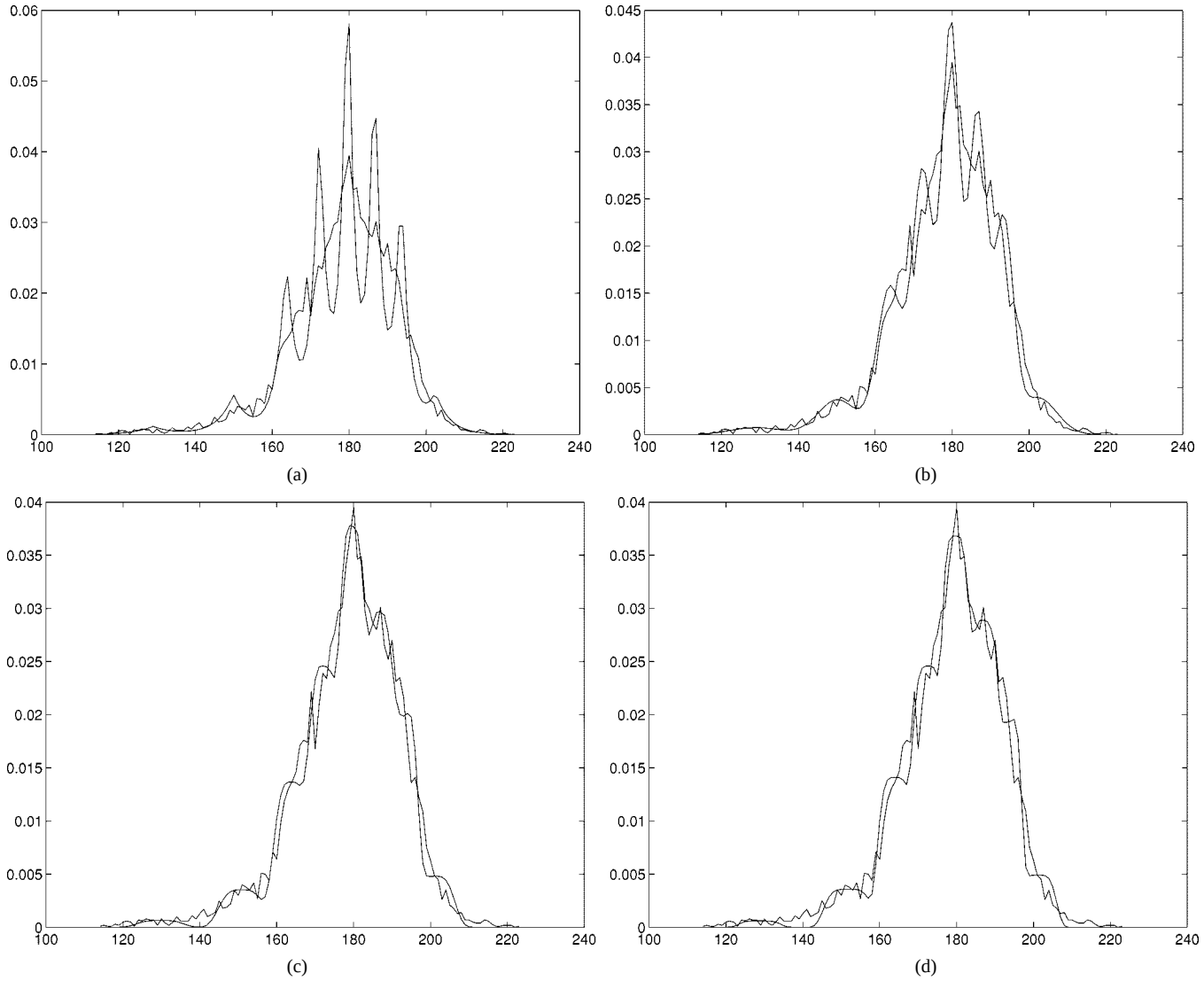

Fig. 7. Comparison of learning curves and histogram of the original mammogram with different α, $k = 8$. The optimal $\alpha = 3.0$. (a) $\alpha = 1.0$, GRE $= 0.0783$. (b) (a) $\alpha = 2.0$, GRE $= 0.0369$. (c) $\alpha = 3.0$, GRE $= 0.0251$. (d) $\alpha = 4.0$, GRE $= 0.0282$.

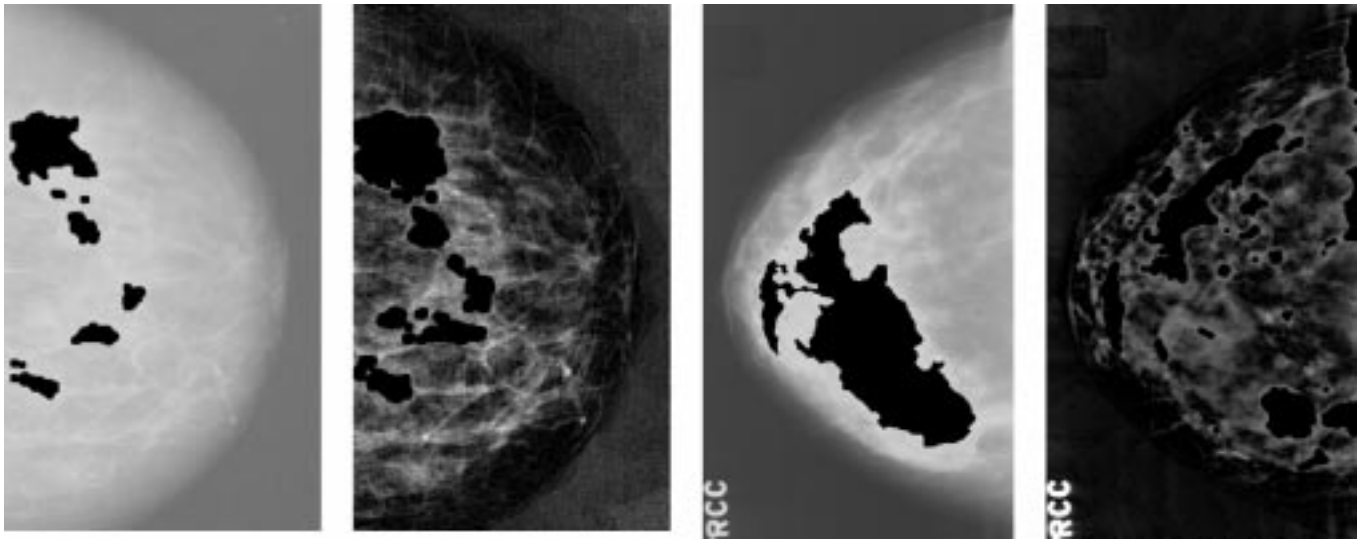

Fig. 8. Suspected mass segmentation results based on the original mammogram. (b) Result based on the enhanced mammogram, $K = 4$, $\alpha = 3.0$. (c) and (d) Results based on another original mammogram and its enhanced image.

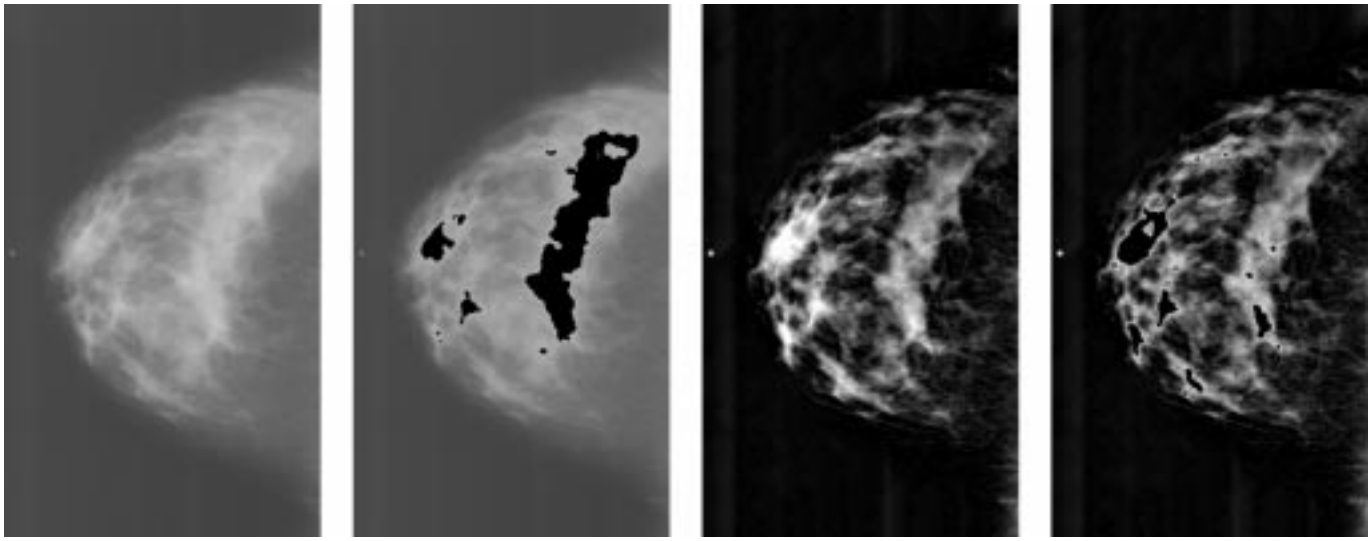

(a) (b) (c) (d)

Fig. 9. Examples of normal mixed fatty and glandular mammogram. (a) Original mammogram. (b) Segmentation result based on the original mammogram. (c) Enhanced mammogram. (d) Result based on the enhanced mammogram, $k = 4$, $\alpha = 3.0$.

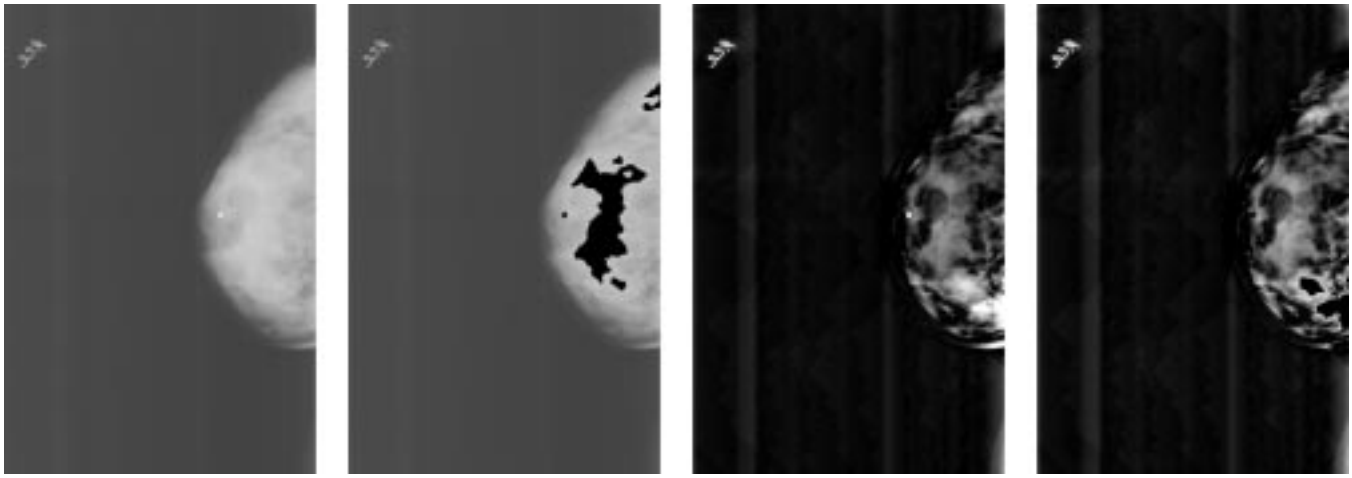

(a) (b) (c) (d)

Fig. 10. Examples of normal dense mammogram. (a) Original mammogram. (b) Segmentation result based on the original mammogram. (c) Enhanced mammogram. (d) Result based on the enhanced mammogram, $k = 4$, $\alpha = 3.0$.

this measure links the image text and its sample averages. Our experience has suggested that this post-segmentation measure may be a suitable objective criterion for evaluating the quality of image segmentation in a fully unsupervised situation [22], [26]–[28]. Table V shows our evaluation data from three different segmentation methods when applied to the real images.

Performance of Combined Morphological Filtering and Model-Based Segmentation using a Larger Database: The proposed segmentation method was used to extract suspicious mass regions from the 200 testing mammograms. Without enhancement, a total of 1142 potential mass regions were isolated including 114 of the 186 true masses. With enhancement, a total of 3143 potential mass regions were extracted including 181 of the 186 true masses. The results demonstrated that more true masses were picked up after enhancement although more false cases were also included. The undetected areas mainly occurred at the lower intensity side of the shaded objects or obscured by fibroglandular tissues that, however, were extracted on morphological enhanced mammograms. In addition, when the margins of masses are ill defined, only parts of suspicious masses were extracted from the original mammograms. For the purpose of "lesion site selection," we believe that the sensitivity should be the sole criterion for the performance evaluation of the method. We have 181/186 versus 114/186. Our method is unsupervised and automatic and does not involve any detection effort at this moment. To our best knowledge, there is no objective criterion available for the evaluation of image enhancement performance before a detection effort is involved. We only claimed that the enhancement step is important and effective with respect to the purpose of "lesion site selection."

Fig. 8 demonstrates some segmentation results based on the original and enhanced mammograms. We compared the segmentation results based on the enhanced mammogram ($K = 4$, and $\alpha = 3.0$) with those based on the original mammogram ($K = 8$, and $\alpha = 3.0$) as shown in Fig. 8. Comparing the results in Fig. 8(b) with those in Fig. 8(a), we can see that after

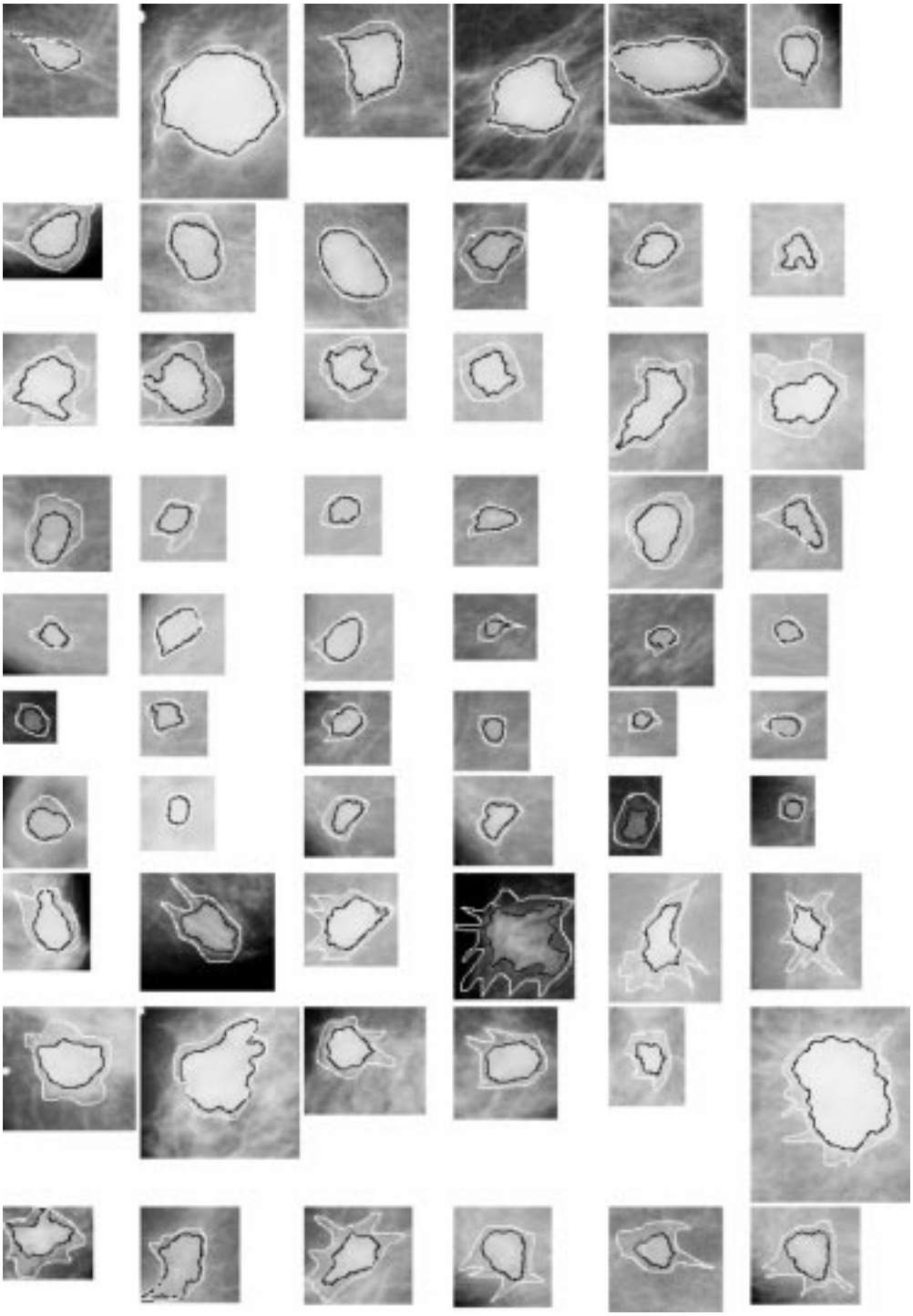

Fig. 11. Comparison results of segmantation based on the enhanced mammograms. Black outlines denote the computer-segmented result. White outlines denote ther radiologist-segmanted results.

enhancement, a more accurate region was detected for the suspected mass which has ill-defined margin. Getting an accurate suspected region is a crucial issue since geometric features are extracted based on suspected regions and these features are very important for further true mass detection. In addition, we observed that one suspected mass was missed in Fig. 8(a) but was detected in Fig. 8(b). As we have mentioned in Section I, none of the suspected masses should be missed in the segmentation step. Fig. 8(c) and (d) demonstrate the segmentation of a suspected mass that lies in dense breast tissue. As shown in Fig. 8(c), the whole fibroglandular tissue area was segmented when based on the original mammogram. After enhancement, the suspected region was segmented exactly as shown in Fig. 8(d).

We have also included the segmentation results on the normal mammograms. Fig. 9 demonstrate the segmentation results based on the original and enhanced mixed fatty and glandular mammograms. Fig. 10 demonstrate the segmentation results based on the original and enhanced dense mammograms. We

would like to emphasize that the objective of this paper is to provide a segmentation technique which can enhance and extract potential mass site from the background so that the characterization of the related mass pattern can be accurately extracted in terms of focused feature selection and analysis. The method of course will produce many mass-like areas, but it will be a plausible outcome since the accurate description of nonmass cases characterized by mass-like sites will benefit the follow-on detection step where the performance of the classifier depends on an accurate separation of mass and nonmass in the featured spaces. The details will be described in [29].

For the purpose of evaluating the performance of the segmentation method, we used both simulated studies and expert visual inspection to validate the methods and results. The radiologist has concluded that the lesion characteristics after the proposed enhancement have been better displayed and all possible lesion areas have been successfully identified. In addition to the visual inspection, we have measured the overlap between the computer-segmented and the radiologist segmented mass regions to evaluate our method. Fig. 11 shows the comparison results of segmentation based on the enhanced mammograms. Fig. 11 includes 60 benign and malignant mass patches which were cut from the whole mammograms after the segmentation. The white outline was drawn by the radiologist while the black outline was produced by the computer and was superimposed upon the original image. As we can see from Fig. 11, for most of cases, the ratio of mutual overlap area of the radiologist segmented mass region and the computer-segmented mass region to the radiologist segmented mass area is large than 50%. In addition, even the poorest result picked the true lesion in the correct location and depicted the characteristics of the mass reasonably. It is important to understand that "lesion area segmentation" is not our objective, so there is no "best" or "worst" segmentation results. Our objective is "lesion site selection" with a possible highest sensitivity through a global unsupervised enhancement and segmentation scheme.

V. Conclusion

In this paper, we propose a combined method of using morphological operations, a FGGM modeling, and a CBRL to enhance and segment various breast tissue textures and suspicious mass lesions from mammographic images. This phase is a crucial step in mass detection for an improved CAD. We emphasized the importance of model selection which includes the selection of the number of image regions K and the selection of FGGM kernel shape controlled by α. The experimental results indicate that the suspected masse sites selection can be affected by different K and α. We proposed the EM algorithm together with the information theoretic criteria to determine the optimal K and α. With optimal K and α, the segmentation results can be significantly improved. We also showed that with the proposed pattern-dependent enhancement algorithm using morphological operations, the subtle masses can be segmented more accurately than those when the original image is used for extraction without enhancement. To summarize, the morphological filtering enhancement combined with the stochastic model-based segmentation is an effective way to extract mammographic suspicious patterns of interest, and thereby may facilitate the overall performance of mammographic CAD of breast cancer.

Acknowledgment

The authors would like to thank Z. Gu of the Lombardi Cancer Center and I. Sesterhenn of the Armed Forces Institute of Pathology for their scientific input on the knowledge of cell oncology and pathology, and R. Shah MD, Director of Breast Imaging, BAMC for his evaluation of cases to our database.

References

[1] H. Kobatake, M. Murakami, H. Takeo, and S. Nawano, "Computerized detection of malignant tumors on digital mammograms," *IEEE Trans. Med. Imag.*, vol. 18, pp. 369–378, May 1999.

[2] R. Zwiggelaar, T. C. Parr, J. E. Schumm, I. W. Hutt, C. J. Taylor, S. M. Astley, and C. R. M. Boggis, "Model-based detection of spiculated lesions in mammograms," *Med. Image Anal.*, vol. 3, no. 1, pp. 39–62, 1999.

[3] M. A. Kupinski and M. L. Giger, "Automated seeded lesion segmentation on digital mammograms," *IEEE Trans. Med. Imag.*, vol. 17, pp. 510–517, Aug. 1998.

[4] N. Karssemeijer and G. M. te Brake, "Detection of stellate distortions in mammogram," *IEEE Trans. Med. Imag.*, vol. 15, pp. 611–619, Oct 1996.

[5] W. K. Zouras, M. L. Giger, P. Lu, D. E. Wolverton, C. J. Vyborny, and K. Doi, "Investigation of a temporal subtraction scheme for computerized detection of breast masses in mammograms," *Excerpta Medica*, vol. 1119, pp. 411–415, 1996.

[6] N. Petrick, H. P. Chan, B. Sahiner, and D. Wei, "An adaptive density-weighted contrast enhancement filter for mammographic breast mass detection," *IEEE Trans. Med. Imag.*, vol. 15, no. 1, pp. 59–67, 1996.

[7] M. Sameti and R. K. Ward, "A fussy segmentation algorithm for mammogram patttion," in *Digital Mammgraphy*. ser. International Congress Series, K. Doi, Ed. Amsterdam, The Netherlands: Elsevier, 1996, pp. 471–474.

[8] W. P. Kegelmeyer Jr., J. M. Pruneda, P. D. Bourland, A. Hillis, M. W. Riggs, and M. L. Nipper, "Computer-aided mammographic screening for spiculated lesions," *Radiology*, vol. 191, pp. 331–337, 1994.

[9] F. F. Yin, M. L. Giger, C. J. Vyborny, K. Doi, and R. A. Schmidt, "Comparison of bilateral-subtraction and single-image processing techniques in the computerized detection of mammographic masses," *Investigat. Radiol.*, vol. 28, no. 6, pp. 473–481, 1993.

[10] B. Zheng, Y. H. Chang, and D. Gur, "Computerized detection of masses in digitized mammograms using single-image segmentation and a multilayer topographic feature analysis," *Acad. Radiol.*, vol. 2, pp. 959–966, 1995.

[11] H. D. Li, M. Kallergi, L. P. Clarke, V. K. Jain, and R. A. Clark, "Markov random field for tumor detection in digital mammography," *IEEE Trans. Med. Imag.*, vol. 14, pp. 565–576, Sept. 1995.

[12] M. L. Giger, C. J. Vyborny, and R. A. Schmidt, "Computerized characterization of mammographic masses: Analysis of spiculation," *Cancer Lett.*, vol. 77, pp. 201–211, 1994.

[13] T. K. Lau and W. F. Bischof, "Automated detection of breast tumors using the asymmetry approach," *Comput. Biomed. Res.*, vol. 24, no. 9, pp. 1501–1513, 1995.

[14] M. J. Bianchi, A. Rios, and M. Kabuka, "An algorithm for detection of masses, skin contours, and enhancement of microcalcifications in mammograms," in *Proc. , Symp. Computer Assisted Radiology*, Winston-Salem, NC, June 1994, pp. 57–64.

[15] T. Lei and W. Sewchand, "Statistical approach to x-ray CT imaging and its application in image analysis–Part II: A new stochastic model-based image segmentation technique for x-ray CT image," *IEEE Trans. Med. Imag.*, vol. 11, pp. 62–69, Feb. 1992.

[16] Y. Wang, T. Adali, and S.-C. B. Lo, "Automatic threshold selection using histogram quantization," *SPIE J. Biomedical Optics*, vol. 2, no. 2, pp. 211–217, April 1997.

[17] J. Zhang and J. W. Modestino, "A model-fitting approach to cluster validation with application to stochastic model-based image segmentation," *IEEE Trans. Pattern Anal. Machine Intell.*, vol. 12, pp. 1009–1017, Oct. 1990.

[18] H. Li, K. J. R. Liu, Y. Wang, and S. C. Lo, "Morphological filtering and stochastic modeling-based segmentation of masses on mammographic images," in *Proc. IEEE Nuclear Science Symp. Medical Imaging Conf.*, 1996, pp. 1792–1796.

[19] J. Serra, *Image Analysis and Mathematical Morphology*. London, U. K.: Academic, 1982.

[20] A. P. Dempster, N. M. Laird, and D. B. Rubin, "Maximum likelihood from incomplete data via the EM algorithm," *J. Roy. Statist. Soc. Ser. B*, vol. 39, pp. 1–38, 1977.

[21] Y. Wang, T. Adali, C. M. Lau, and S. Y. Kung, "Quantitative analysis of MR brain image sequences by adaptive self-organizing finite mixtures," *J. VLSI Signal Processing*, vol. 18, no. 3, pp. 219–240, 1998.

[22] Y. Wang, T. Adali, S. Y. Kung, and Z. Szabo, "Quantification and segmentation of brain tissues from MR images: A probabilistic neural network approach," *IEEE Trans. Image Processing*, vol. 7, pp. 1165–1181, Aug. 1998.

[23] H. Akaike, "A new look at the statistical model identification," *IEEE Trans. Automat. Contr.*, vol. 19, no. 6, pp. 716–723, 1974.

[24] J. Rissanen, "Modeling by shortest data description," *Automat.*, vol. 14, pp. 465–471, 1978.

[25] R. A. Hummel and S. W. Zucker, "On the foundations of relaxation labeling processes," *IEEE Trans. Pattern Anal. Machine Intell.*, vol. 5, pp. 267–286, Mar. 1983.

[26] A. Hoover, G. J. Baptoste, X. Jiang, P. J. Flynn, H. Bunke, D. B. Goldgof, K. Bowyer, D. W. Eggert, A. Fitzgibbon, and R. B. Fisher, "An experimental comparison of range image segmentation algorithms," *IEEE Trans. Pattern Anal. Machine Intell.*, vol. 18, pp. 673–688, July 1996.

[27] Y. J. Zhang, "A survey on evaluation methods for image segmentation," *Pattern Recogn.*, vol. 29, no. 8, pp. 1335–1346, 1996.

[28] A. M. Bensaid, L. O. Hall, J. C. Bezdek, L. P. Clarke, M. L. Silbiger, J. A. Arrington, and R. F. Murtagh, "Validity-guided clustering with applications to image segmentation," *IEEE Trans. Fuzzy Syst.*, vol. 4, pp. 112–123, May 1996.

[29] H. Li, Y. Wang, K. J. R. Liu, S.-C. B. Lo, and M. T. Freedman, "Computerized Radiographic Mass Detection—Part II: Decision Support by Featured Database Visualization and Modular Neural Networks," *IEEE Trans. Med. Imag.*, vol. 20, no. 4, pp. 302–313, Apr. 2001.